Naoya SODA, Hiroshi ADACHI

Ibaraki University

Iron loss analysis of EI-shaped iron-core inductor considering vector magnetic property

Abstract. *We analyze the EI-shaped iron-core inductors with air-gaps by using 2-D finite element analysis considering vector magnetic property. We can investigate the iron loss distribution in the cores affected by the length of the air-gaps. As a result, we can show the difference of local iron loss distribution in the inductor cores when the length of the air-gaps is changed. Moreover, it is shown that the iron loss distribution differs from the maximum flux density distribution.*

Streszczenie. *Przeanalizowano rdzeń typu EI metopdą elementu skończonego z uwzględnieniem właściwości wektorowych. Zbadano wpływ wielkości szczeliny. Stwierdzono różny rozkład lokalnej wartości strat zależny od wielkości szczeliny. Ten rozkład styrat zależy też od wielkości indukcji. (**Analiza strat w rdzeniu typu EI z uwzględnieniem właściwości wektorowych**)*

Keywords: finite element analysis, inductor, iron loss, vector magnetic property.
Słowa kluczowe: analiza pola magnetycznego, straty.

Introduction

The important problems in inductors are high efficiency and saving energy. The two main types of inductor are air-core inductors and iron-core inductors. When high inductance is necessary, the EI-shaped iron-core inductor with air-gaps as shown in Fig.1 is generally used. In the case of the EI-shaped iron-core inductor, the inductance is often changed by an adjustment of the length of the air-gaps. Therefore, from the point of view of saving energy, it is very important to investigate the iron loss distribution in the cores when the length of the air-gaps is changed. In order to investigate the iron loss distribution in the cores, there are some methods to measure directly the iron loss, for example, by using the needle probe method [1]. However, when the inductor cores are very small as shown in Fig. 1, it is impossible to measure the iron loss distribution in the cores by using the method above.

On the other hand, because the E-core is punched to E-shape from one grain-oriented silicon steel sheet, the magnetic properties in the core are strongly affected by the magnetic anisotropy of the steel sheet and the field strength vector $\boldsymbol{H}$ is not parallel to the flux density vector $\boldsymbol{B}$. In this case, an analysis using only the magnetic properties of the rolling direction and the transverse direction is not able to consider correctly the phase difference between the vectors $\boldsymbol{B}$ and $\boldsymbol{H}$. In addition, because the fringing flux occurs at the air-gaps of the iron-core inductors, the alternating flux inclined from the rolling direction and the elliptic rotating flux occur in the cores. Therefore, it is very effective to investigate the inductor cores by the magnetic field analysis considering the two-dimensional (2-D) vector magnetic property [2, 3].

In this paper, we analyze the EI-shaped iron-core inductors with air-gaps by using 2-D finite element analysis with the E&S model [3]. The E&S model can express the vector magnetic property of both the alternating and the rotating magnetic flux conditions by using the vector relationship between the vectors $\boldsymbol{B}$ and $\boldsymbol{H}$ during one period. As a result, we can investigate the iron loss distribution in the cores when the length of the air-gaps is changed. Moreover, we construct the inductors, and measure the voltage-current characteristics in order to compare with the analysis results.

Magnetic field analysis

We have carried out the 2-D finite element analysis with the E&S model, which is expressed as follows:

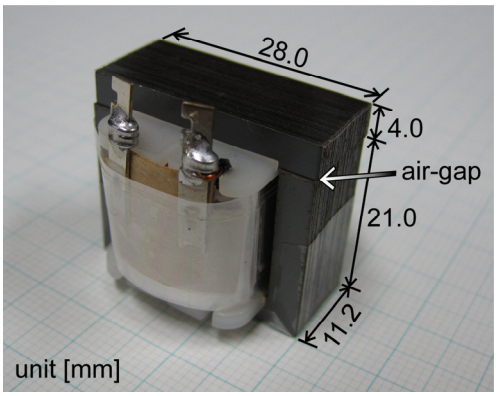

Fig.1. EI-shaped iron-core Inductor

$$\text{(1)}\quad \begin{cases} H_x = \nu_{xr} B_x + \nu_{xi} \dfrac{\partial B_x}{\partial \tau} \\ H_y = \nu_{yr} B_y + \nu_{yi} \dfrac{\partial B_y}{\partial \tau} \end{cases}$$

where ν_{xr} and ν_{yr} are named as the magnetic reluctivity coefficient, ν_{xi} and ν_{yi} are named as the magnetic hysteresis coefficient, τ is in a range from 0 to 2π. The ν_{xr}, ν_{xi}, ν_{yr} and ν_{yi} are expressed as follows:

$$\text{(2)}\quad \begin{cases} \nu_{xr} = k_{xr1} + k_{xr2} B_x^2 + k_{xr3} B_x \left(\dfrac{\partial B_x}{\partial \tau} \right) + k_{xr4} \left(\dfrac{\partial B_x}{\partial \tau} \right)^2 \\ \nu_{xi} = k_{xi1} + k_{xi2} B_x^2 + k_{xi3} B_x \left(\dfrac{\partial B_x}{\partial \tau} \right) + k_{xi4} \left(\dfrac{\partial B_x}{\partial \tau} \right)^2 \\ \nu_{yr} = k_{yr1} + k_{yr2} B_y^2 + k_{yr3} B_y \left(\dfrac{\partial B_y}{\partial \tau} \right) + k_{yr4} \left(\dfrac{\partial B_y}{\partial \tau} \right)^2 \\ \nu_{yi} = k_{yi1} + k_{yi2} B_y^2 + k_{yi3} B_y \left(\dfrac{\partial B_y}{\partial \tau} \right) + k_{yi4} \left(\dfrac{\partial B_y}{\partial \tau} \right)^2 \end{cases}$$

where the coefficients k_{xrn}, k_{xin}, k_{yrn} and k_{yin} (n=1, 2, 3, 4) are calculated from the measured data by using the 2-D vector magnetic measurement [3, 4].

From the Maxwell's equations and the E&S model (1), the governing equation in the 2-D quasi-static magnetic field can be written as follows:

$$\frac{\partial}{\partial x}\left(\nu_{yr}\frac{\partial A}{\partial x}\right)+\frac{\partial}{\partial y}\left(\nu_{xr}\frac{\partial A}{\partial y}\right)+\frac{\partial}{\partial \tau}\left\{\frac{\partial}{\partial x}\left(\nu_{yi}\frac{\partial A}{\partial x}\right)+\frac{\partial}{\partial y}\left(\nu_{xi}\frac{\partial A}{\partial y}\right)\right\}=-J_0 \quad (3)$$

where $A(=A_z)$ is the magnetic vector potential, J_0 is the exciting current density. Additionally, we assume the eddy current loss is included in the vector magnetic property. Because the components of reluctivity coefficients ν_{xr}, ν_{xi}, ν_{yr} and ν_{yi} have nonlinearity, it is necessary to calculate iteratively until those values become constant. We can carry out the nonlinear magnetic field analysis considering the vector magnetic property.

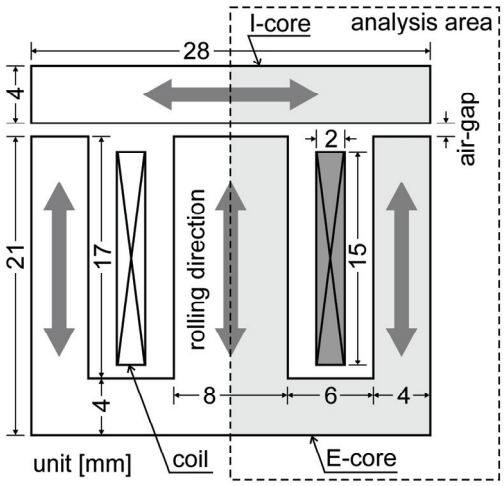

Fig.2. Analysis model of EI-shaped iron-core inductor

Fig. 2 shows the analysis model of EI-shaped iron-core inductor. The arrows in the cores indicate rolling direction. A half of the region is analyzed because the inductor model has symmetry. The lengths of three air-gaps between E-core and I-core are equal as shown in Fig. 2.

In this analysis, we assume that the current waveform is a perfect sine waveform. Therefore, the terminal voltage of inductor is calculated from the magnetic vector potential A as follows:

$$V = 2\int_{C_f}\frac{\partial A}{\partial t}ds + R_c\frac{J_0 S_c}{N_c} \quad [\mathrm{V}] \quad (4)$$

where C_f is the contour along the winding in finite element region, R_c is the resistance of the winding coil, S_c is the cross-sectional area of the winding coil, N_c is the number of turns.

Next, we calculate distribution of the iron loss in the cores. The iron loss of a finite element can be calculated directly from the vectors $\boldsymbol{B}$ and $\boldsymbol{H}$ of analysis results by the following equation:

$$P_t = \frac{1}{\rho T}\int_0^T\left(H_x\frac{dB_x}{dt}+H_y\frac{dB_y}{dt}\right)dt \quad [\mathrm{W/kg}] \quad (5)$$

where ρ is the core material density and T is the period of the exciting waveform. Therefore, the total iron loss of the inductor can be calculated by the following equation:

$$P_{\mathrm{total}} = 2\left(\rho\cdot D_p\cdot N_{os}\cdot\sum_{i=1}^{N_{es}}P_{ti}\cdot S_i\right) \quad [\mathrm{W}] \quad (6)$$

where D_p is the thickness of the steel sheet, N_{os} is the number of laminations of the steel sheet, N_{es} is the number of finite elements in the cores, P_{ti} is the iron loss of a finite element, and S_i is the area of a finite element. In addition, the total iron loss is doubled because the analytical area is a half of the inductor as shown in Fig. 2.

Measurement results

In this paper, it is difficult to measure directly the iron loss distribution in the cores because the inductors are very small as shown in Fig. 1. Therefore, in order to compare with the analysis results, we construct the inductors and measure the voltage-current characteristics. We construct four kinds of inductors with different air-gap length. The inductors are one inductor without air-gap, and three inductors with air-gap length of 0.01, 0.025, and 0.05mm. The air-gap length is adjusted by inserting a thin insulator sheet with the same thickness as the gap length in the air-gap. In the case without air-gap, no insulator sheet is inserted in the air-gap. The cores of inductors consist of the grain-oriented silicon steel sheet (RG11) of 0.35mm thickness, and the total number of laminations is 32. The number of coil turns is 72. The frequency of power supply is 50Hz. The values of voltage and current are indicated by RMS.

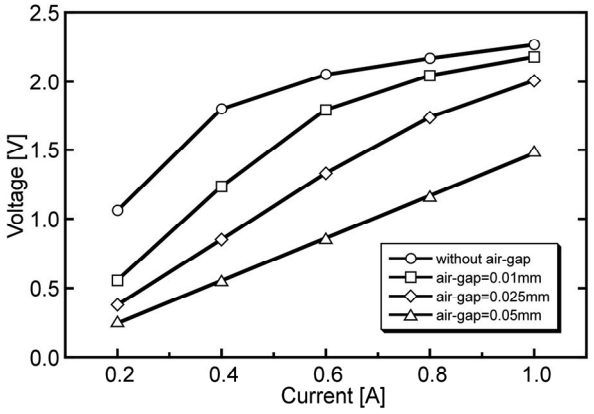

Fig.3. Measured voltage-current characteristics

Fig. 3 shows the measured voltage-current characteristics of the inductors without air-gap, and with air-gap length of 0.01, 0.025, and 0.05mm. We construct four inductors for each gap length and average the voltage-current characteristics. As shown in Fig. 3, as taking air-gap length large, the characteristics exhibit linearity because magnetization saturation in the cores becomes gradually hard. Moreover, when terminal voltage exceeds 2V, the voltage is saturated under the influence of magnetization saturation.

Table 1. The relative errors between the measured voltages and the analyzed voltages for the same current values

	0.2A	0.4A	0.6A	0.8A	1.0A
without air-gap (0.001mm)	24.5%	2.63%	3.96%	0.39%	0.92%
0.01mm	62.1%	9.22%	5.92%	5.03%	3.65%
0.025mm	58.2%	22.1%	4.68%	3.25%	4.49%
0.05mm	36.6%	18.0%	7.69%	2.67%	5.48%

Analysis results and discussion

We analyze the EI-shaped iron-core inductor model shown in Fig. 2. In this analysis, the core material is assumed as the grain-oriented silicon steel sheet (35G155) that has the characteristics similar to RG11.

An imperceptible air-gap remains between E-core and I-core even if we construct the inductor without air-gap. Therefore, in this analysis, we analyze the inductor with air-gap length of 0.001mm instead of analyzing the inductor without air-gap.

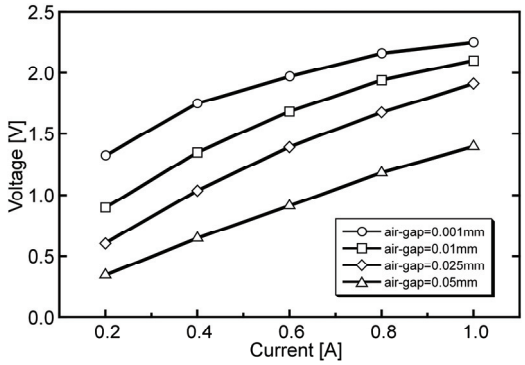

Fig.4. Analyzed voltage-current characteristics

Fig. 4 shows the voltage-current characteristics calculated by (4) from analyzed results, and Table 1 shows the relative errors between the measured voltages shown in Fig. 3 and the analyzed voltages shown in Fig. 4 for the same current values. In this analysis, we used the vector magnetic property that is more than 0.4T. Therefore, we suppose that the large calculation errors occur at 0.2A because the reluctivity data less than 0.4T are calculated by extrapolation. As shown in Fig. 4 and Table 1, analyzed results except 0.2A are similar to measured ones.

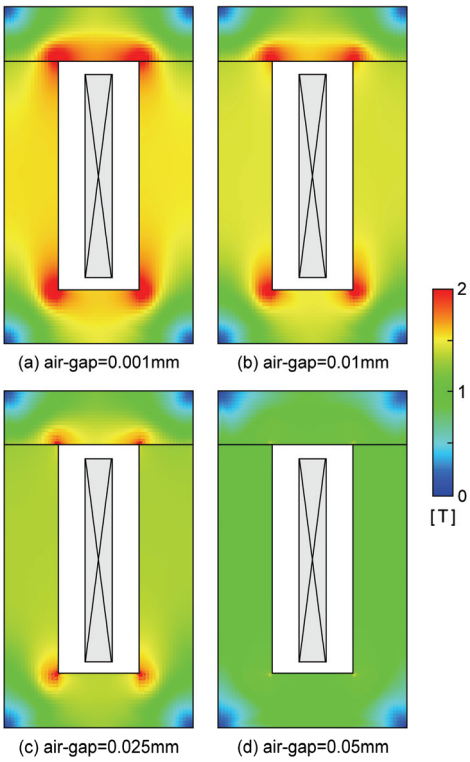

Fig.5. Maximum flux density distribution in the cores under the current 1.0A

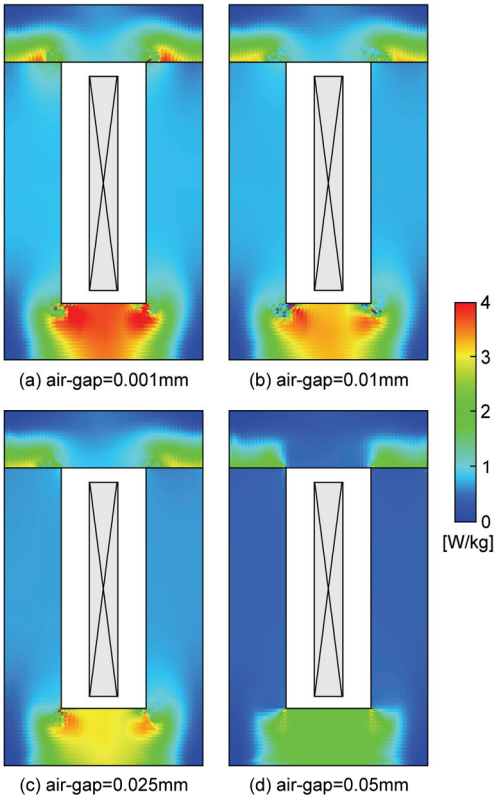

Fig.6. Iron loss distribution in the cores under the current 1.0A

Figs. 5 and 6 show the maximum flux density distribution and the iron loss distribution in the cores under the current 1.0A, respectively.

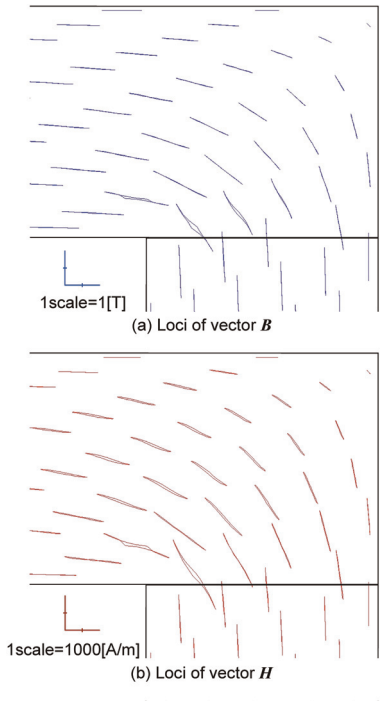

Fig.7. Distribution of the loci of the vectors $\boldsymbol{B}$ and $\boldsymbol{H}$ near the air-gap (air-gap length=0.01mm, current=1.0A)

Though the maximum flux density is large at only four corners in the core, the iron loss distribution is quite different from the maximum flux density distribution. Fig. 6

represents that it is impossible to calculate an iron loss distribution from a maximum flux density distribution. As shown in Fig. 6, In the E-cores, large iron loss occurs at the area magnetized perpendicularly to the rolling direction. Since the magnetization saturation occurs from the inner side of corner, the iron loss becomes especially large there. In the I-cores, because magnetic flux bends near air-gaps when magnetic flux flows into the I-core from the E-core, large iron loss occurs near air-gaps. Fig. 7 shows distribution of the loci of the vectors $\boldsymbol{B}$ and $\boldsymbol{H}$ near the air-gap between E-core and I-core. In Fig. 7, the air-gap length is 0.01mm and the current is 1.0A. As shown in Fig. 7 (a), the alternating flux inclined from the rolling direction and the elliptic rotating flux occur in the I-core. Moreover, because many rotating fields occur at the corner part in the I-core as shown in Fig. 7 (b), the iron loss becomes large there as shown in Fig. 6 (b).

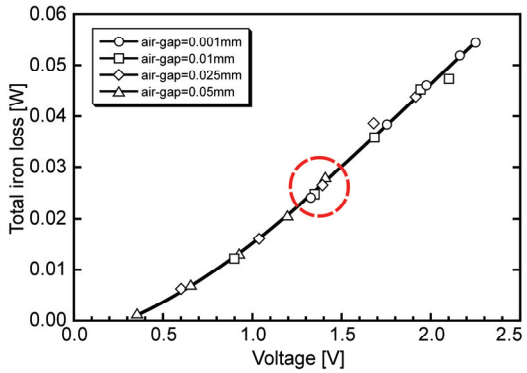

Fig.8. Relationship of total iron loss of the inductors to the voltage

Next, we calculate the total iron loss of the inductors by (6) from the local iron loss distribution as shown in Fig. 6. Fig. 8 shows the relationship of the total iron loss to the terminal voltage. In this analysis, the terminal voltage represents the average magnetic flux in the inductor. When the air-gap length is enlarged, the average magnetic flux in the inductor decreases and the total iron loss also decreases. Therefore, as shown in Fig. 8, the values of total iron loss of the inductors with different air-gap length are almost on the same curve. The total iron loss is the average value and is hard to reflect the variation of local iron loss. We compare the local iron loss distribution under the comparatively similar voltage surrounded with the circle dashed line in Fig. 8.

Fig. 9 shows the iron loss distribution of the inductor with different air-gap length under the comparatively similar voltage. As shown in Figs. 9 (a) and (b), when the air-gap length is small, the iron loss is large at the inner side of corner in the E-core. On the other hand, as shown in Fig. 9 (d), when the air-gap length is large, large value of iron loss is distributed widely near the air-gap in the I-core. As a result, we can investigate the difference of local iron loss distribution in the inductor cores when the length of the air-gaps is changed.

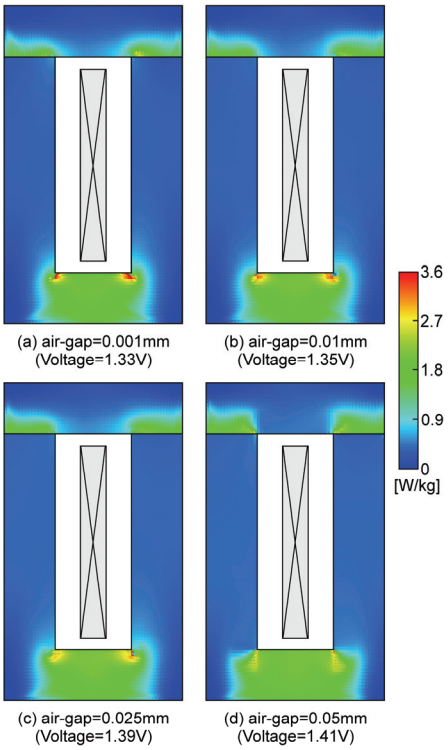

Fig.9. Iron loss distribution in the cores under the comparatively similar voltage

Conclusion

In this paper, we analyze the EI-shaped iron-core inductors with air-gaps by using 2-D finite element analysis with the E&S model and obtain the iron loss distribution in the cores when the length of the air-gaps is changed.

It is shown that the iron loss distribution differs from the maximum flux density distribution. Therefore, it is very important to obtain the iron loss distribution directly by using magnetic field analysis with the E&S model considering vector magnetic property.

Moreover, we can show the difference of local iron loss distribution in the inductor cores when the length of the air-gaps is changed.

REFERENCES

[1] Hashimoto Y., Enokizono M., Mogi H., Measurement of the localized iron loss in electromagnetic steel sheet by using the needle probe method, *Journal of Applied Physics*, 91(2002), No. 10, 6935-6937

[2] Zhang Y., Eum Y. H., Xie D., Koh C. S., An Improved Engineering Model of Vector Magnetic Properties of Grain-Oriented Electrical Steels, *IEEE Trans. on Magn.*, 44(2008), No. 11, 3181-3184

[3] Soda N., Enokizono M., Improvement of T-Joint Part Constructions in Three-Phase Transformer Cores by Using Direct Loss Analysis with E&S Model, *IEEE Trans. on Magn.*, 36(2000), No. 4, 1285-1288

[4] Soda N., Enokizono M., E&S hysteresis model for two-dimensional magnetic properties, *Journal of Magnetism and Magnetic Materials*, 215-216(2000), 626-628

***Authors**: dr. Naoya SODA, Department of Electrical and Electronic Engineering, College of Engineering, Ibaraki University, Hitachi, Ibaraki, 316-8511 Japan, E-mail: soda@mx.ibaraki.ac.jp*